

Multiparametric MRI mapping of oxygen delivery and hypoxia in renal 786-O-R murine xenografts

James PB O'Connor¹, Yann Jamin², Jessica KR Boulton², Muhammad Babur³, John C Waterton¹, Damien McHugh¹, Andrew R Reynolds⁴, Kaye J Williams³, Geoff JM Parker¹, and Simon P Robinson²

¹Imaging Sciences, University of Manchester, Manchester, Greater Manchester, United Kingdom, ²Radiotherapy and Imaging, Institute of Cancer Research, Sutton, London, United Kingdom, ³School of Pharmacy, University of Manchester, Manchester, Greater Manchester, United Kingdom, ⁴Breakthrough Breast Cancer Research Centre, Institute of Cancer Research, Sutton, London, United Kingdom

Intended Audience: Basic scientists and clinicians with interest in tumor hypoxia, radiobiology, radiotherapy and hypoxia-modifying agents.

Introduction: MRI mapping of tumor oxygen delivery and hypoxia is an unmet clinical need¹. T₁-weighted oxygen enhanced MRI (OE-MRI) can distinguish well oxygenated voxels from those that are hypoxic²; blood oxygenation level dependent (BOLD) imaging can quantify the oxygen binding to haemoglobin after gas challenge³; and dynamic contrast enhanced MRI (DCE-MRI) estimates of perfusion have variable relationships to tissue and genetic hypoxia markers^{4,5}. We show that combining these 3 methods enables detailed MRI evaluation of tumor oxygen delivery and hypoxia.

Methods: Cells from a sunitinib resistant 786-O renal carcinoma xenograft (786-O-R) were cultured in RPMI + 10% fetal calf serum treated with antibiotics. Tumors were propagated by injecting 3 x 10⁶ cells in 100µl of sterile PBS into the flanks of female SCID mice. Single slice MRI data were acquired on a 7T horizontal bore Bruker system after localization with T₂-w images. Anaesthetized mice were positioned in a 3-cm birdcage coil. Tumors were immobilized using a jig and gas delivery was at 2 l/min via a nosepiece. Warm air maintained the animal core temperature at 37 °C.

One multi-gradient echo image (to map R₂^{*}) and two True-FISP inversion recovery images (to map R₁) were acquired on medical air (21% O₂), using sequences described previously⁶. Voxel size was 0.234 x 0.234 x 1.0 mm.

Four inversion recovery images were acquired during the first 10 minutes of 100% O₂ gas breathing "wash-in" (each taking 2.5 mins). Then one R₁ map and one R₂^{*} map were acquired (identical to initial images on medical air). Finally, 0.1 mmol/kg gadopentetate (GD) was injected and True-FISP DCE-MRI was collected (10 s temporal resolution) (Figure 1).

Voxel-wise R₂^{*}, R₁ and IAU_{C60} were derived for each map, using a Bayesian maximum *a posteriori* approach, with in-house software⁶. ΔR₂^{*} was calculated by R₂^{*} (O₂) - R₂^{*} (air). ΔR₁ was calculated with R₁ (O₂) data from the final R₁ map and the mean of the two R₁ maps acquired on air breathing.

Intraperitoneal injection of pimonidazole (60mg/kg) occurred 55 minutes before 100% O₂ inhalation began. Hoechst 33342 (15mg/kg) was administered by tail vein injection one minute prior to cull. Hypoxic fraction (HF) and perfused vessel area (PVA) were calculated from 5 µm cryostat sections.

Results and Discussion: Nine mice were imaged. Tumor size (range 178 to 815 mm³) had no significant relationship to any functional MRI data.

Summary OE-MRI and DCE-MRI data: All tumors showed overall positive R₁ increase, with average ΔR₁ = 0.120 s⁻¹ (range 0.012 to 0.201). Within-scan R₁ co-efficient of variation (CoV) was 0.72%. Based on this, individual voxels with R₁ change greater than 2 x (CoV) x (mean baseline tumor R₁) were considered statistically different from baseline. Tumor IAU_{C60} values average = 0.139 mmol.min (range 0.0203 to 0.404). PVA correlated with median ΔR₁ (Spearman's rho 0.905, p=0.002), the % of voxels with positive ΔR₁ (rho 0.857, p=0.007) and median IAU_{C60} (rho 0.893, p=0.007). The HF was correlated to median ΔR₁ (rho -0.783, p=0.013) and the % of voxels with positive ΔR₁ (rho -0.801, p=0.010).

Voxel-wise analysis of heterogeneity: ΔR₁ and IAU_{C60} maps were divided into voxels demonstrating positive enhancement or not. OE-MRI positive ΔR₁ was defined as above. DCE-MRI enhancement was defined as IAU_{C60} > 0. Maps of OE-MRI and DCE-MRI signal mismatch were created to evaluate spatial heterogeneity of oxygen delivery and hypoxia. Analysis revealed four distinct voxel categories: 1) **well perfused and well oxygenated**, 2) **avascular with oxygen build up**, 3) **perfused but hypoxic** and 4) **avascular and no oxygen delivery**. In 6 of the 7 tumors with paired OE-MRI and DCE-MRI data, well perfused, well oxygenated voxels were located in the tumor periphery and central avascular areas were surrounded by a transition zone of hypoxia (example images in Figure 2). Well perfused voxels had greater positive ΔR₁ than the avascular voxels with oxygen build up (p<0.001 at all four dynamic time points) and reached plateau within 2.5 mins. Avascular voxels with oxygen build up reached plateau only by 7.5 mins. Perfused but hypoxic voxels became progressively more negative in ΔR₁ values, with significance (p<0.001) reached at 7.5 mins (Figure 2).

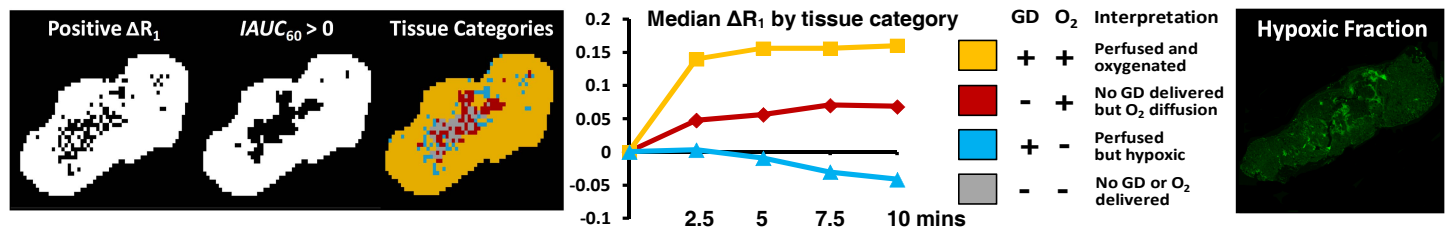


Figure 2 (left): Example maps of O₂ and GD enhancement along with mismatch; (middle): Dynamic ΔR₁ onset and magnitude during 100% O₂ wash in (avascular anoxic category omitted) and interpretation of multi-parametric signal changes; (right): Pimonidazole adduct formation

Relationship of ΔR₂^{*} to other MRI parameters: Average median ΔR₂^{*} was -18.7 ms⁻¹. Median ΔR₂^{*} had no consistent relationship to ΔR₁ or IAU_{C60} and did not relate to PVA or HF on pathology. However, when the voxel-wise ΔR₂^{*} was analyzed in each tumor region parcellated by OE-MRI and DCE-MRI, greatest ΔR₂^{*} were seen in hypoxic tumor regions (median ΔR₂^{*} -19.0 ms⁻¹) and this distribution of voxel values was significantly different from all other tumor voxel categories defined on OE-MRI and DCE-MRI (Figure 3).

Conclusion: The multi-parametric data presented provide new insight into the spatial and temporal relationships between regional perfusion and hypoxia in tumors. This method has potential for non-invasive delineation of tumor hypoxic volume for radiotherapy and monitoring response to radiotherapy and hypoxia-modifying agents.

References: ¹Tatum (2006), Int J Rad Biol 82:699-757; ²Linnik (2014), MRM doi: 10.1002/mrm.24826; ³Baker (2013), IJROBP 87:160-167; ⁴Ceelan (2006) IJROBP 64:1188-1196; ⁵Halle (2012), Can Res 72:5285-5295; ⁶Burrell (2013), JMRI 38:429-434.

Grant support: Cancer Research UK (CRUK) Clinician Scientist award; CRUK and EPSRC Cancer Imaging Centre funding; and Wellcome Trust.

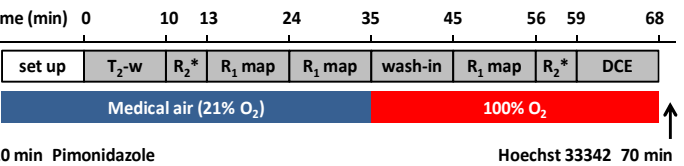


Figure 1: Data collection, gas administration and pathology schedule

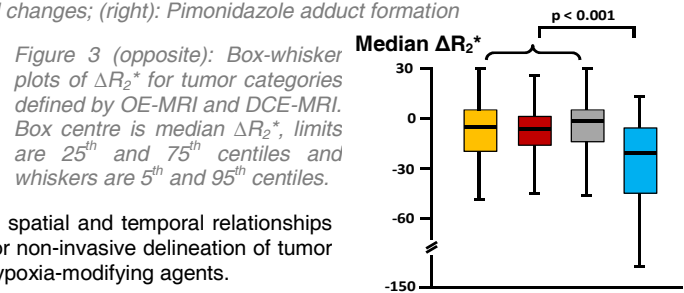


Figure 3 (opposite): Box-whisker plots of ΔR₂^{*} for tumor categories defined by OE-MRI and DCE-MRI. Box centre is median ΔR₂^{*}, limits are 25th and 75th centiles and whiskers are 5th and 95th centiles.